



Characterization of PEO/PVP/GO nanocomposite solid polymer electrolyte membranes: microstructural, thermo-mechanical, and conductivity properties

H. K. Koduru¹ · F. Scarpelli² · Y. G. Marinov³ · G. B. Hadjichristov³ · P. M. Rafailov³ · I. K. Miloushev³ · A. G. Petrov³ · N. Godbert² · L. Bruno⁴ · N. Scaramuzza^{1,5}

Received: 29 November 2017 / Revised: 8 January 2018 / Accepted: 3 February 2018 / Published online: 13 March 2018

© Springer-Verlag GmbH Germany, part of Springer Nature 2018

Abstract

Poly (ethylene oxide) (PEO)/polyvinylpyrrolidone (PVP) blended nanocomposite polymers, incorporating graphene oxide (GO) nano-sheets and embedded with NaIO₄ salt, were prepared using solution casting technique. The as-prepared nanocomposite electrolyte membranes were characterized by SEM, TEM, XRD, and Raman vibrational spectroscopic techniques to confirm the dispersion of GO nano-sheets and to understand the synergistic properties of GO/polymer interactions as a function of GO nano-sheets concentration. GO fillers incorporated electrolyte membranes demonstrated distinctive surface morphology composed of circular-shaped protuberances of different dimensions. The decrease of Raman intensity ratio (I_D/I_G) and in-plane crystallite size (L_a) values of the nanocomposites suggested the good dispersion and confinement of the GO nano-sheets. The optical properties of blend electrolyte films were studied as a function of GO filler concentration using optical absorption and diffuse reflectance spectra. In reference to PEO/PVP/NaIO₄, the resultant PEO/PVP/NaIO₄/GO (0.4% in weight) electrolyte membrane demonstrated both an increase in tensile strength of ca. 42% and in Young's modulus of ca. 40%, improvements coupled with a maximum fractured elongation of 3%. Through impedance spectroscopy analysis, the role of the GO nano-sheets onto the room temperature conductivity properties of the prepared electrolyte membranes has been probed.

Keywords Nanocomposite polymer electrolytes · Transmission electron microscopy · Vibrational spectroscopy · Raman studies · Stress-strain studies and thermal stability properties

Electronic supplementary material The online version of this article (<https://doi.org/10.1007/s11581-018-2484-8>) contains supplementary material, which is available to authorized users.

✉ H. K. Koduru
koduruharika@gmail.com

¹ Dipartimento di Fisica, Università degli Studi della Calabria, Via P. Bucci, Cubo 33B, 87036 Rende (CS), Italy

² MAT-INLAB (Laboratorio di Materiali Molecolari Inorganici), Dipartimento di Chimica e Tecnologie Chimiche, Università della Calabria, 87036 Arcavacata di Rende (CS), Italy

³ Georgi Nadjakov Institute of Solid State Physics, Bulgarian Academy of Sciences, 72 Tzarigradsko Chaussee Blvd., 1784 Sofia, Bulgaria

⁴ Department of Mechanical, Energy and Management Engineering–DIMEG, University of Calabria, Via P. Bucci, Cubo 44C, 87036 Rende (CS), Italy

⁵ CNISM—Unità di Ricerca di Cosenza c/o Dipartimento di Fisica, Università degli Studi della Calabria, Via P. Bucci, Cubo 31C, 87036 Rende (CS), Italy

Introduction

The substantial global energy demand for advanced electrical energy storage devices continues to stimulate researchers for the development of advanced energy storage systems. Rechargeable alkali metal-ion batteries (Li⁺, Na⁺, Mg²⁺, ... etc.) are recognized as promising energy sources to power the portable consumer electronic devices (mobile phones, notebooks, personal computers, and digital cameras), electric or hybrid electric vehicles, and solar energy storage devices [1, 2]. In this context, the development of novel electrolyte systems, which are ionically conductive and constitute the core of efficient batteries, is crucial to fulfill the present technological requirements of the medium- and large-scale batteries. Among liquid and gel electrolytes, solid polymer electrolytes (SPEs) have attracted ever-increasing interest owing to their several advantages, such as lower cost, improved safety features,

solvent-free material, excellent flexibility, and easy process [3, 4]. Polyethylene oxide (PEO) is one of the promising and ion-conductive semi-crystalline polymer. PEO is characterized by a high dielectric constant, flexible ethylene oxide segments, enabling PEO to solvate different inorganic salts at high concentration levels [5]. However, pure PEO-based SPEs demonstrate poor ionic conductivities at room temperature, which prevent their use as key components in the fabrication of secondary ion batteries, electrochromic devices, solar cells, and sensors [6, 7]. Several approaches have been attempted to enhance the room temperature ionic conductivity of PEO-based SPEs through addition of ionic liquids, cross-linking, inclusion of low molecular weight plasticizers, incorporation of nanostructured materials, and blending with plastic crystal materials [8–10]. However, blending polymers seems to be one of the versatile approaches to fabricate PEO-based SPEs with desirable characteristics. Indeed, this method can allow using high molecular weight crystalline polymers in conjunction with high molecular weight amorphous polymers to confer to the resulting blend with higher solubility in organic solvents as well as higher affinity with inorganic salts. For this purpose, polyvinylpyrrolidone (PVP) is one of the more promising conjugated amorphous polymer since its amorphous matrix can support faster ionic mobility compared to other semi-crystalline polymers. Indeed, the presence of carbonyl groups ($-C=O$) within the PVP side chains enable to coordinate cations of a wide variety of inorganic salts providing free mobile ions into the electrolytic system [11]. From a practical application point of view, polymer electrolytes must fulfill the following requirements: (i) a high ionic conductivity, (ii) an appreciable mechanical strength, (iii) a good thermal stability, and (iv) a wide electrochemical stability window [12, 13]. Fabrication of SPEs displaying all the above-mentioned features is not an easy task, but using nanocomposite polymer electrolytes could represent the best option to reach such a goal and develop novel efficient electrolyte systems. Furthermore, polymer composites reinforced with inorganic fillers of nanometer range dimensions have recently attracted great interest due to the unexpected synergistic properties resulting from the combination of the two components [14]. In particular, the incorporation of nano-size fillers (zinc oxide, alumina, titania) into PEO matrix has drawn significant attention for the improvement of the electrical performance without sacrificing the mechanical strength of the material [15, 16]. In this perspective, carbon-based nano-additives-doped PEO electrolytes can be considered as a new class of materials with multifunctional properties [17]. It is worth to mention that, in comparison to inorganic nano-dimensional fillers, carbon-based nano-fillers have an exceptional combination of thermal, mechanical, and electrical properties that make them unique candidates to choose to fabricate versatile nanocomposites

SPEs [18]. Graphene oxide (GO) is a hydrophilic layered material, an oxidized graphene derivative, containing oxygen-bearing functional groups on its edges and basal planes. Interestingly, GO additives can readily be dispersed without precipitation and swelled in water or polar solvents, allowing when dispersed into a polymer to form a high number of EO/GO interfaces through intercalation of the polymer chains into the gallery of GO [19, 20]. Polymer/GO nanocomposites are characterized by improved electrical, thermal, and mechanical properties compared to either the matrix or to the conventional composites. They are commonly referred as particulate micro-composites, because of their unique phase morphology deriving from layer intercalation and/or exfoliation that maximizes interfacial contact between the organic and inorganic phases that in turn enhances the bulk properties [21]. Several studies have been reported on the influence of GO additives onto the structural, thermal, and electrical properties of lithium salt complexes of pure PEO-based SPEs [22, 23]. Understanding the compatibility and specific mechanisms responsible for the formation of profound GO/polymer interfaces when GO nano-additives are used in blended SPEs would open a new window to study the electrochemical, thermal, optical, dimensional, and mechanical stability properties of PEO blend-based nanocomposite SPEs.

To date, most of the research work that reported on lithium salt complexes of PEO-based SPEs is dedicated to lithium-ion rechargeable battery (LIB) applications, owing to their high energy density and long life cycle values compared to all other battery chemistries [24]. However, high cost, decrease of abundance, environmental impact, and safety limitations are impeding LIBs widespread implementation in large-scale batteries for future generation technologies [25]. Such impediment shows the necessity to search for alternative energy storage system technology capable of complementing the LIB technology. Among the accessible battery chemistries, sodium-based rechargeable batteries (SIBs) have recently captured much attention for their environmentally friendly and non-toxic features and low cost due to the natural abundance [26]. In this light, the present report is dedicated to study GO nano-sheets incorporated and $NaIO_4$ salt complexed (PEO/PVP) nanocomposite blend electrolyte membranes using various characterization techniques. For this purpose, a combination of transmission electron microscopy (TEM), scanning electron microscopy (SEM), Micro Raman, UV-Vis-NIR diffuse reflectance (DRS), differential scanning calorimetry (DSC), thermogravimetric analysis (TGA), tensile strength, and EIS analysis measurements were performed to understand the synergistic effect of the constituents onto the physico-chemical, thermomechanical stability and ionic conductivity properties of fabricated PEO/PVP/ $NaIO_4$ /GO nanocomposite polymer electrolyte membranes.

Experimental section

Materials

Polyethylene oxide (PEO, MW = 5,000,000), polyvinylpyrrolidone (PVP, MW = 360, 000), aqueous graphene oxide (GO) solution (2 mg/ml), sodium metaperiodate (NaIO_4) salt of analytical grade, and methanol (99.8%) were purchased from Sigma Aldrich and used without any further chemical purification. In its crystalline state, PEO polymer backbone contains seven structural units ($\text{CH}_2\text{--CH}_2\text{--O}$) and two helical turns per fiber with an identity period of 1.93 nm (Scheme 1a). PVP is an amorphous and easily soluble polymer in polar solvents. The primitive pyrrolidone ring in PVP polymer is shown in (Scheme 1b). GO nano-sheets are constituted of a layered graphene structure, GO layers being embedded with terminal edge carboxyl groups (Scheme 1c).>

Preparation of PEO/PVP/ NaIO_4 /GO electrolyte membranes

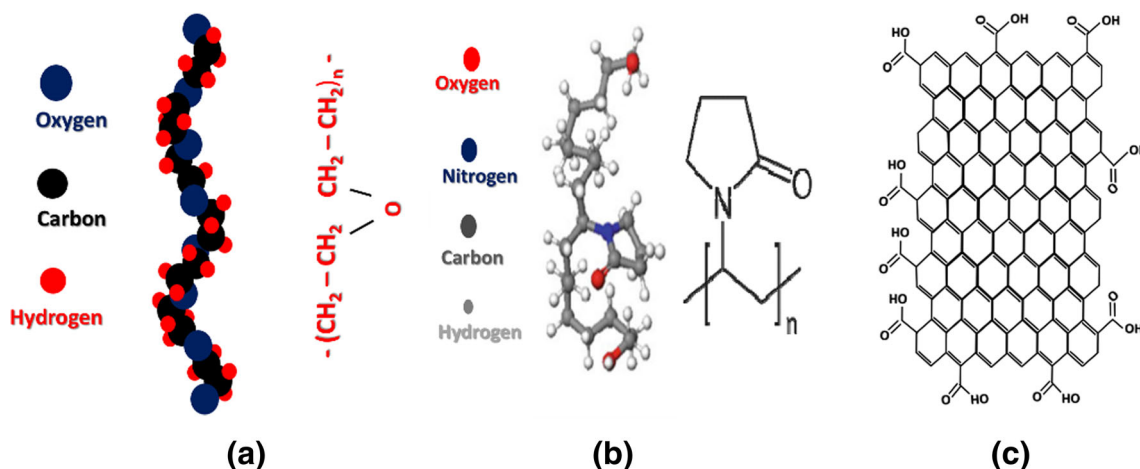
The PEO/PVP/ NaIO_4 /GO nanocomposite electrolyte membranes were prepared by using a solution casting technique (as illustrated in Scheme 2). Initially, PEO/PVP (70/30 w/w) blend mixture solution was prepared as described in our previous work [27] and in the next step, individually prepared NaIO_4 salt solution (10 w/w) and aqueous GO solutions of varying concentrations (0.2, 0.4, and 0.6 w/w) were simultaneously added dropwise to the as-prepared PEO/PVP blend solutions. The mixture was rapidly stirred continuously for 10 h to insure the homogeneous dispersion of GO nano-sheets, obtaining in the end a viscous slurry PEO/PVP/ NaIO_4 /GO electrolyte solution. The resultant nanocomposite viscous slurry solution was transferred to polypropylene dishes and allowed to dry at 40 °C for 4 days in enclosed environment (to minimize the surface skin effect) in order to

harvest uniform free-standing nanocomposite polymer electrolyte membranes of thickness $\sim 150 \mu\text{m}$.

Characterization

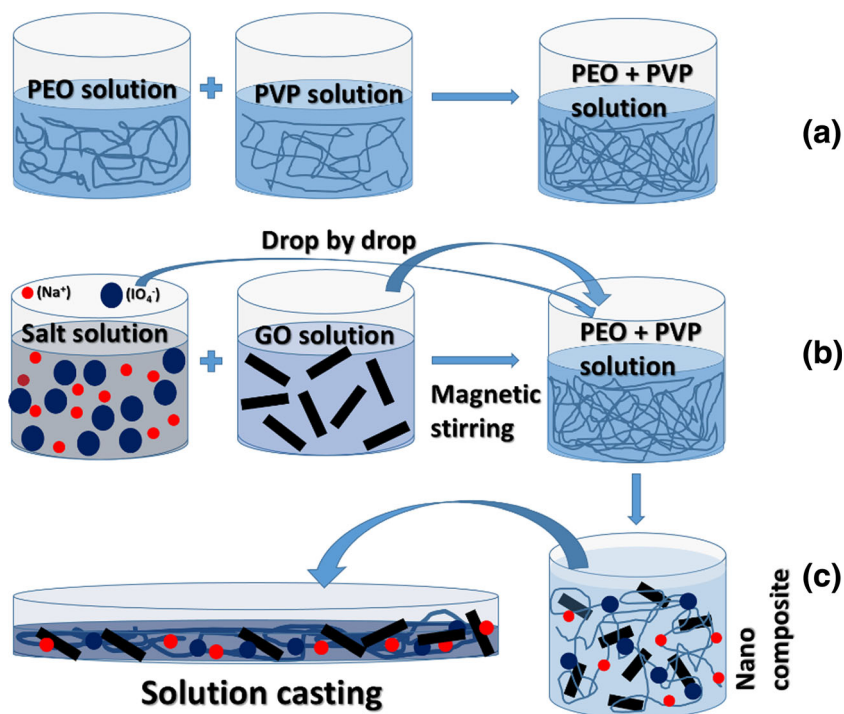
The surface morphologies of GO-loaded polymer electrolyte membranes were observed by SEM using a JSM 5500 instrument under an acceleration voltage of 15 kV. SEM images were taken at room temperature by depositing a thin gold layer over surfaces of the samples using box coater RF sputtering technique. Measurements by transmission electron microscopy (TEM) (HR STEM JEOL JEM 2100, acceleration voltage 80–200 kV, maximum resolution, 0.23 nm) were carried out to understand the distribution of incorporated GO nano-sheets in the matrices of electrolyte membranes. To prepare the samples for TEM measurements, methanol was employed as a solvent to control the morphology of individual PEO, PVP polymers on GO nano-sheets, and allow simultaneous observation of polymers and GO. The resultant solutions were dipped using a copper grid which was dried under ambient condition for observation. This approach was specifically effective for polymer matrices incorporated with low concentrations of GO substances.

X-ray diffraction patterns (XRD) were obtained at room temperature using a X-ray diffractometer (Bruker, D8 ADVANCE) with $\text{Cu K}\alpha$ radiation ($\lambda = 0.154 \text{ nm}$). The samples were scanned in the 2θ range of $10^\circ\text{--}80^\circ$ with a constant step width of 0.02° and at counting time of 35 s/step. Raman spectroscopic measurements were performed on a HORIBA Jobin Yvon Labram HR visible spectrometer equipped with a Peltier-cooled CCD detector. For these measurements, He-Ne ($\lambda = 663 \text{ nm}$) laser beam was focused on a spot of size about $2 \mu\text{m}$ over the surface of the samples using microscope optics and recorded micro-Raman spectra in the wavenumber region of $200\text{--}2000 \text{ cm}^{-1}$. Optical absorption spectra were recorded at room temperature using a Perkin Elmer Lambda 1050 UV-Vis spectrophotometer (equipped with an integrating sphere)



Scheme 1 Schematic representations of **a** crystalline PEO, **b** PVP molecule, and **c** graphene oxide (GO) structure

Scheme 2 **a** Preparation of PEO/PVP blend polymer solution by mixing individually dissolved PEO and PVP polymers. **b** Preparation of nanocomposite blend solution by incorporation of salt ions and GO additives in drop by drop method. **c** Solution casting of nanocomposite solution to get solid electrolyte membranes



in the wavelength range of 250–2500 nm. Diffuse optical reflectance spectra of all blend electrolyte membranes were recorded at room temperature using a Carry 500 UV-Vis-NIR double-beam spectrophotometer (equipped with an integrating sphere) in the wavelength range of 300–2500 nm.

The thermal properties of all samples were studied using a Netzsch DSC 204F1 Phoenix DSC under nitrogen atmosphere. In all thermal scans, weights of electrolyte samples loaded aluminum pans, empty aluminum pan (as reference), and lids were recorded. DSC thermograms of all electrolyte samples were obtained in the temperature range from 60 to 300 °C at a scan rate of 10 °C/min. The glass transition temperature (T_g) was determined from the inflection point of the transitions. Other thermal parameters, such as the melting temperature (T_m) and melting enthalpy (ΔH_m), were estimated as well. Decomposition temperature analyses were conducted under a nitrogen atmosphere by using a TGA Q50 TA thermogravimetric analyzer with a programmed heating rate of 10 °C min⁻¹ from 30 to 800 °C. The mechanical properties of pure and nanocomposite electrolyte membranes were determined by tensile strength measurements using an electro-mechanical universal testing machine (MTS Criterion, model 42) equipped with a 100 N load cell. The fixture used for fitting the specimen on the machine is the MTS vise action grips (model 100) with a load capacity of 100 N, which accommodates testing electrolyte membranes with a section up to 2 mm thick and 10 mm wide. A potentiostat/galvanostat (SP-200, Biologic) was utilized to record the impedance spectra in the frequency range of 0.1 Hz–1 MHz. The electrochemical impedance spectroscopy technique was employed to

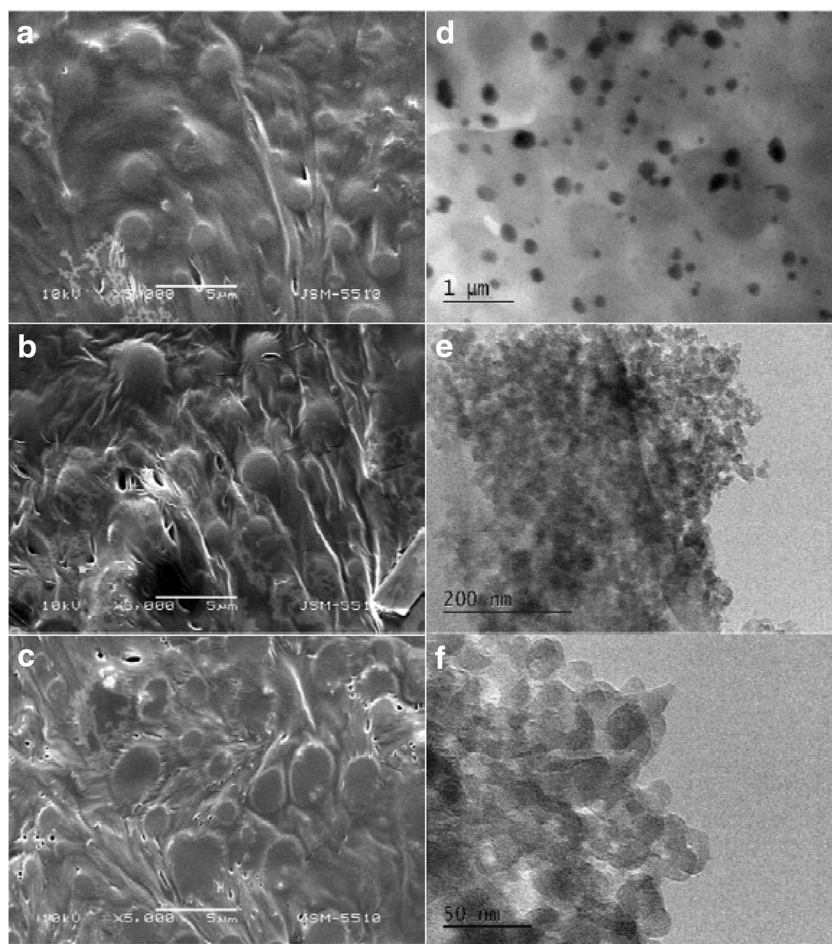
estimate the room-temperature ionic conductivity values of all fabricated SPEs. In this case, the electrolyte membranes were sandwiched between two circular-shaped aluminum electrodes (1 cm × 1 cm) and the entire assembly was placed in closed chamber.

Results and discussion

SEM and TEM studies

SEM and TEM studies were carried out to observe the effect of the presence of the GO nano-sheets onto the surface morphological features of membranes and check the dispersion quality of the GO nano-sheets within the matrices of PEO/PVP/NaIO₄ electrolyte membranes (Fig. 1). Comparatively, nanocomposite PEO/PVP/NaIO₄/GO electrolyte membranes demonstrated a moderately rough surface morphology characterized by circular-shaped protuberances of different dimensions associated to the GO nano-sheets (Fig. 1a–c). The presence of homogeneously dispersed protuberances could be evidenced for the good dispersion and substantial confinement of GO nano-sheets within the polymer matrix. This kind of microstructures reveal the enhancement in density of polymer/GO interfaces and the effect of articulated confinement of GO nano-sheets on the segmental motion of PEO chains [28]. The inclusion and intercalation of exfoliated GO nano-sheets in the polymeric matrices of fabricated blend electrolytes were further confirmed by TEM measurements (Fig. 1d–f). In the nanocomposite electrolyte membranes, the GO nano-sheets

Fig. 1 Scanning electron microscopy images for GO nano-sheets incorporated PEO/PVP/NaIO₄ electrolytes **a** 0.2 wt%, **b** 0.4 wt%, and **c** 0.6 wt%. Transmission electron microscopy pictures at different magnifications for PEO/PVP/NaIO₄/GO (0.2% in weight) electrolyte (**d–f**)



contribute for the formation of well-interconnected structure within the matrix of blended electrolytes probably due to the presence of the GO carboxyl functional groups. Upon increase of GO concentration, further increase in exfoliation rate and greater compatibility of GO nano-sheets in the matrices of PEO/PVP/NaIO₄ was noticed. This could lead to the increase in integrity of PEO/PVP blend polymer chains around the GO nano-sheets and thus favors for the formation of large number of ether oxygen (EO)/GO interfaces by abridging the randomly inlaid GO nano-sheet in the three-dimensional matrices of nanocomposites.

X-ray diffraction

Figure 2a shows the powder X-ray diffraction (PXRD) patterns of pure and GO-incorporated PEO/PVP/NaIO₄ electrolyte membranes. The PXRD pattern of PEO/PVP/NaIO₄ blend displays several small reflection peaks but is essentially governed by two characteristic reflections at angular positions (in terms of 2θ) of 19.24° and 23.35°, which are associated to the (120) and (112) crystal planes of the PEO monoclinic crystal structure [29]. The incorporation of GO fillers showed the effect in terms of changes in intensity and broadening of the two peaks at

19.24° and 23.35°. These XRD profile modifications could be related to the observation of a synergistic effect of the various functional groups present onto the polymer chains of PEO and PVP and the functionalized carboxylic groups of the GO nano-sheets reducing either the crystallinity of the polymeric blend than preventing the inorganic salt to crystallize, probably by coordination of the Na⁺ ions by the GO carboxylic moieties. This double influence contributes to further disrupt the crystalline helical conformation of PEO thus decreasing its crystallinity and promoting additional amorphousity within the matrix of nanocomposite SPEs [30]. With regard to the PXRD patterns of GO-containing blends, all the small signals at diffraction angles of 12.87, 15.45, 25.78, 27.89, 30.3, and 33.7° (in terms of 2θ), that were already present in the PXRD pattern of the PEO/PVP/NaIO₄ blend, are now consequently clearly distinguishable. Using origin software, the PXRD data of all electrolyte films was fitted by employing Gaussian function and by following peak deconvolution procedures to determine the variation in percentage of crystallinity ($\% \chi_c$) related to PEO/PVP/NaIO₄ (10 wt%) blend electrolytes as a function of GO concentration (Fig. 2b). For comparative investigation, we considered PEO/PVP/NaIO₄ (10 wt%) electrolyte as 100% crystalline polymer blend electrolyte. The relative changes in intensity and/or shift

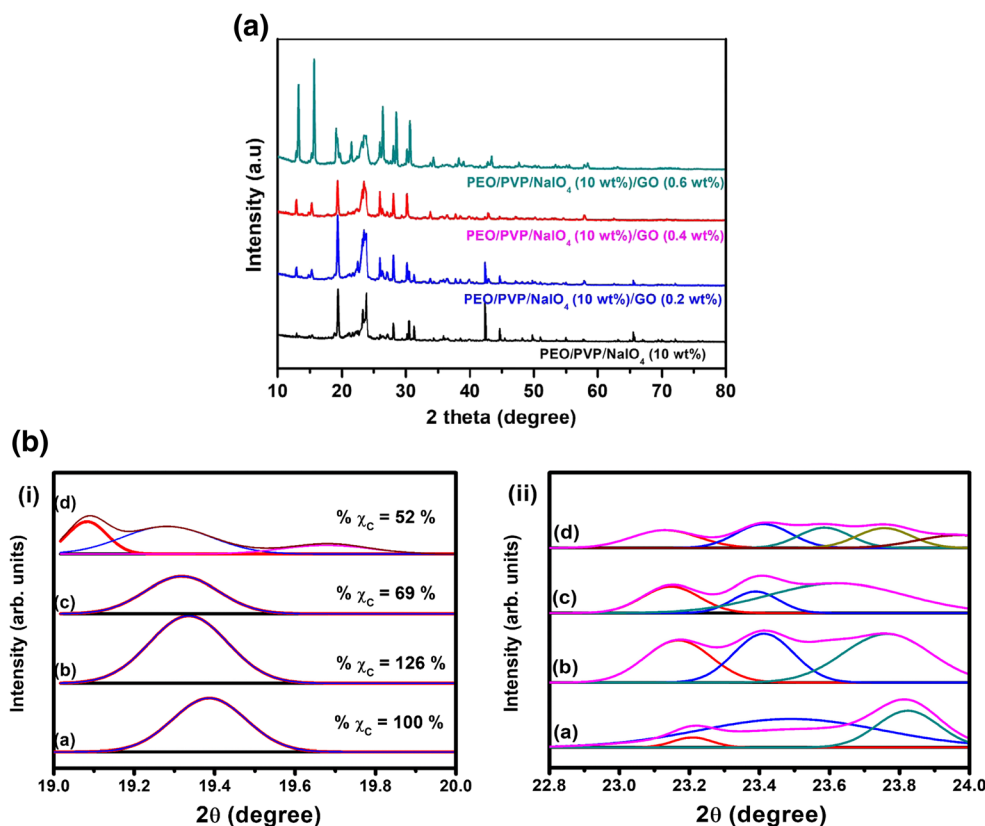


Fig. 2 **a** X-ray diffraction patterns of different polymer electrolyte membranes. **b** (i) The XRD deconvoluted patterns for GO incorporated PEO/PVP/NaIO₄ (10 wt%) electrolyte samples in the 2theta range 19–20°. (a) PEO/PVP/NaIO₄ (10 wt%), (b) PEO/PVP/NaIO₄/GO (0.2 wt%), (c) PEO/PVP/NaIO₄/GO (0.4 wt%), and (d) PEO/PVP/NaIO₄/GO (0.6 wt%). The color of curves indicates as follows: black line: base line, red color: fit peak, blue line: cumulative fit peak. **b** (ii) The XRD

deconvoluted patterns for GO incorporated PEO/PVP/NaIO₄ (10 wt%) electrolyte samples in the 2theta range 22.8–24°. (a) PEO/PVP/NaIO₄ (10 wt%), (b) PEO/PVP/NaIO₄/GO (0.2 wt%), (c) PEO/PVP/NaIO₄/GO (0.4 wt%), and (d) PEO/PVP/NaIO₄/GO (0.6 wt%). The color of curves indicates as follows: black line: base line, red color: first fit peak, blue line: second fit peak, dark cyan: third fit peak, and magenta: cumulative fit peak

in position of crystalline diffraction peak at $2\theta = 19.24^\circ$ suggest the reduction in crystallinity of PEO as a function of salt concentration (Fig. 2b(i)). Noteworthy, XRD patterns of nanocomposites did not display any diffraction peaks related to GO within the range of $2\theta = 10^\circ$ – 80° . This could be due to (i) the intercalation of PEO/PVP blend polymer chains between GO sheets, resulting in increase of GO nano-sheets, and could be beyond the detection range of XRD instrument; (ii) uniform dispersion of exfoliated GO sheets within the matrix of nanocomposites, and thus no diffraction peaks; and/or (iii) could be due to too low concentration GO sheets within the nanocomposites to employ XRD for getting enough diffracted radiation [31].

Raman spectroscopy

Raman spectroscopy has a profound role in the structural characterization of nanocomposite polymer systems, in particular allowing to “visualize” the “GO–polymer chains” interactions, to probe the dynamics of polymer chains as a function of defects on surfaces of GO nano-sheets, and to measure the stacking of the graphene layers and the finite sizes of the crystallites.

The Raman spectra of salt containing PEO/PVP blend electrolyte membrane displayed various characteristic vibrational

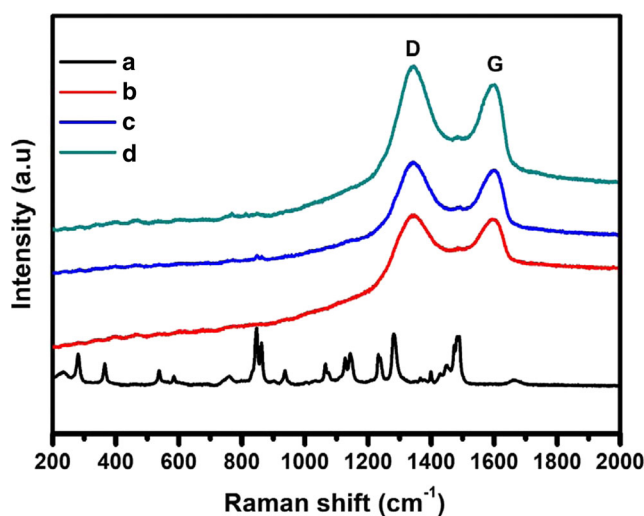


Fig. 3 Raman spectra for (a) PEO/PVP/NaIO₄ (10 wt%), (b) PEO/PVP/NaIO₄ (10 wt%)/GO (0.2 wt%), (c) PEO/PVP/NaIO₄ (10 wt%)/GO (0.4 wt%), and (d) PEO/PVP/NaIO₄ (10 wt%)/GO (0.6 wt%)

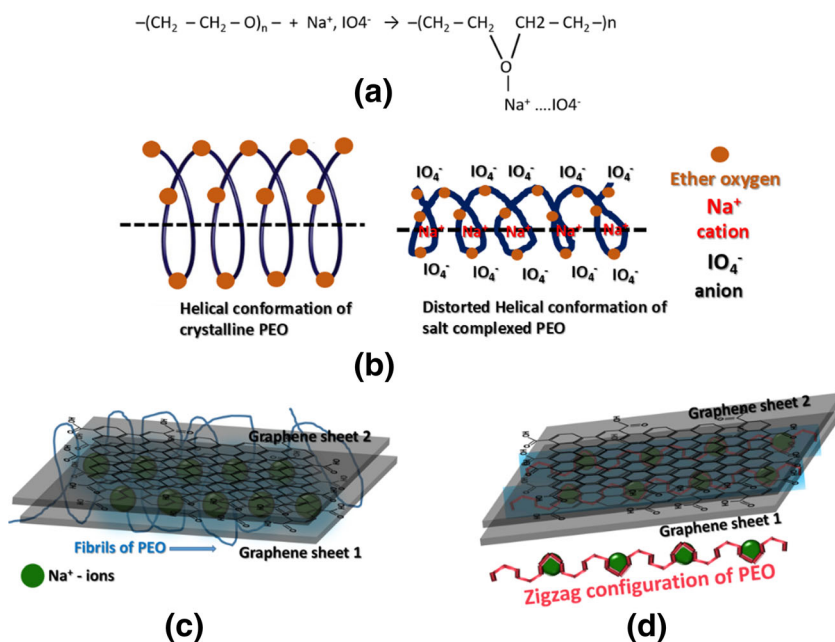
Table 1 Assignments of Raman vibrational bands in the wavenumber range 200–2000 cm^{-1} for various functional groups related to PEO and PVP in blend polymer electrolytes

Raman shift (cm^{-1})	Assignment PEO	Raman shift (cm^{-1})	Assignment PVP
280	$\delta(\text{OCC})_i$ and $\delta(\text{COC})$	–	–
366	$\delta(\text{COC})$ and $\delta(\text{OCC})_i$	–	–
531	$\delta(\text{OCC})_o$	560	N–C=O bend
844	$\gamma(\text{CH}_2)$	754	C–C chain
861	$\gamma(\text{CH}_2)_s$ and $\nu(\text{COC})_s$	851	C–C ring
936	Amorphous	900	C–C ring breathing
1064	$\gamma(\text{CH}_2)_a$ and $\nu(\text{COC})_s$	1023	C–C, CH_2 rock
1077	$\gamma(\text{CH}_2)_s$ and $\nu(\text{COC})_s$	1296	CH_2 wag, C–N stretch
1128	$\nu(\text{COC})_s$	1380	CH bend
1142	$\nu(\text{COC})_a$	1445	CH_2 scissor
1234	$\gamma(\text{CH}_2)_a$	1462	C–N
1280	$\gamma(\text{CH}_2)_s$ and $\gamma(\text{CH}_2)_a$	1494	–
1364	$\omega(\text{CH}_2)_s$ and $\gamma(\text{CC})$	1663	C = O
1396	$\omega(\text{CH}_2)_s$ and $\nu(\text{CC})$	–	–
1445	$\delta(\text{CH}_2)_s$	–	–
1486	$\delta(\text{CH}_2)_s$	–	–

bands in the wavenumber region of 200–2000 cm^{-1} (Fig. 3(a)), which are assigned to different modes of vibrations associated to various functional groups of PEO and PVP polymers (Table 1) [32, 33]. The presence of all characteristic Raman bands related to PEO and PVP polymers evidences for their complete miscibility during the fabrication process of PEO/PVP/NaIO₄ blends. The Raman spectrum of pure GO exhibited two vibrational modes at 1352 and 1584 cm^{-1} , which are associated to D and G bands, respectively (SMI, Fig. S1). The D band is related to structural defects and partially disordered structures of the *sp*² domains and the G band is related to the

E_{2g} vibration mode that originates from the in-plane vibration of *sp*² carbon atoms [34]. Significantly, the characteristic vibrational bands associated to various functional groups of PEO and PVP polymers were strongly suppressed throughout the Raman spectra of nanocomposite electrolyte membranes and the peak head positions of the D and G bands associated to the pristine GO were shifted from 1352 to 1344 cm^{-1} and from 1584 to 1597 cm^{-1} , respectively, due to inclusion of GO nanosheets of different concentrations (Fig. 3(b–d)). These observations suggest the fine dispersion and compatibility of GO nanosheets within the matrix of blended electrolyte; strong

Scheme 3 a Transient cross-link formation between EO molecule of PEO and Na⁺ ions. b Distortion of helical chain of PEO to zigzag configuration due to salt complexation. c Winding of fibrils of PEO around stack of GO sheets. d Intercalation of fibrils of PEO between GO sheets



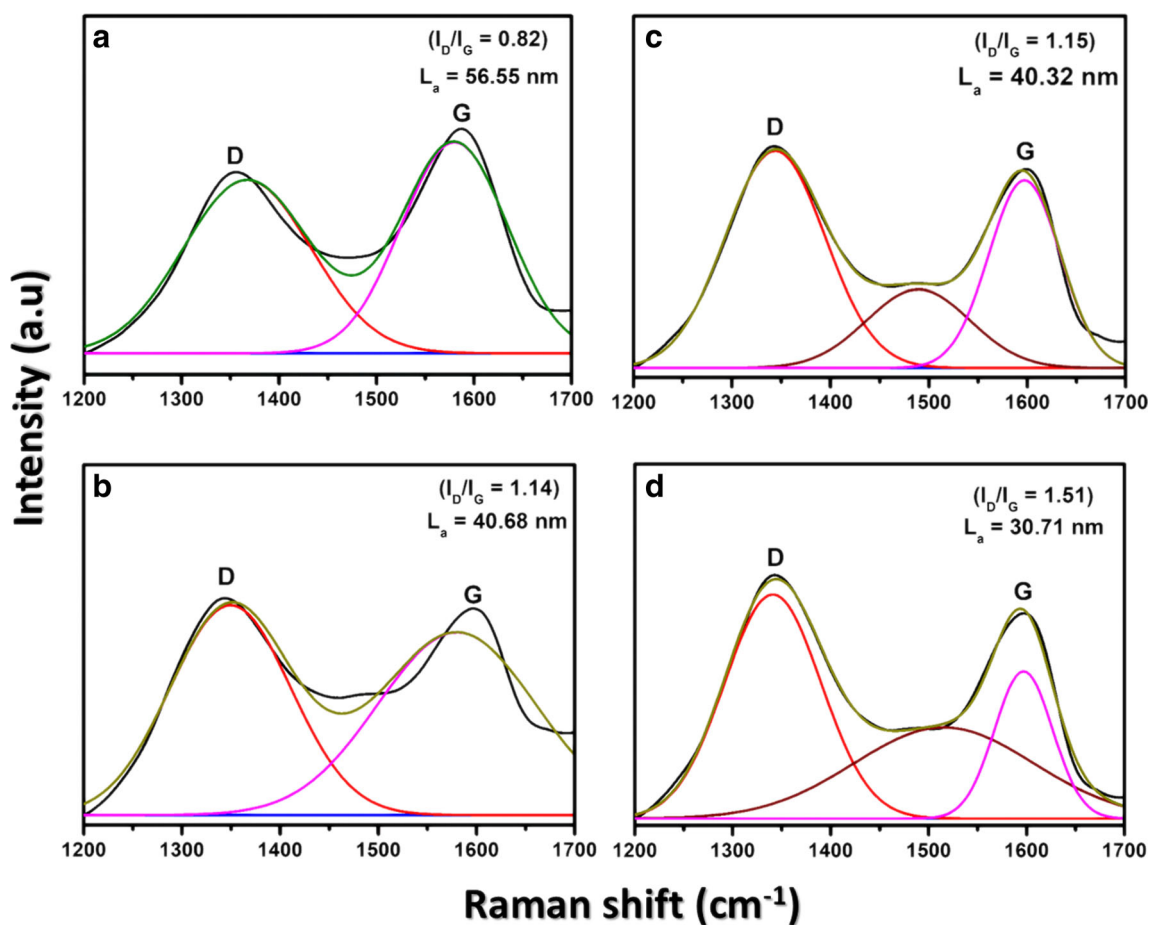


Fig. 4 Deconvolution results of *D* and *G* Raman vibrational bands for **a** pure GO, **b** PEO/PVP/NaIO₄/GO (0.2 wt%), **c** PEO/PVP/NaIO₄/GO (0.4 wt%), and **d** PEO/PVP/NaIO₄/GO (0.6 wt%) nanocomposite

electrolyte membranes. (black line: experimental curve; blue line: base line; red line: first fitted peak; magenta: second fitted peak; and olive: cumulative peak)

intercalation of hydrophilic fibrils of PEO, cations into the gallery of GO; and anchoring of PVP molecules via hydrogen bonding with COO⁻ groups on surface or on edges of the GO nano-sheets (illustrated in Scheme 3) [35].

Generally, Raman intensity ratio of the *D* and *G* bands (I_D/I_G) is a measure of the relative concentration of local defects or disorders in comparison with sp^2 -hybridized graphene domains [36]. The characteristic *D* and *G* bands associated to all nanocomposite electrolyte membranes were fitted by following Gaussian function fitting procedures and estimated “ I_D/I_G ” ratio values with respect to the baseline (Fig. 4a–d). In comparison to pristine GO, an increasing trend of “ I_D/I_G ” values from 0.82 to 1.51 and profile depth between *D* and *G* bands were observed upon increase in weight percentage of GO from 0.2 to 0.6%. These observations could be attributed as follows: (i) increase of the salt dissociation rate and thus increase of transient cross-link formations between the ether oxygens and sodium cations in specific regions (at which GO nano-sheets are not present due to non-uniform distribution of GO nano-sheets) in the matrix of electrolyte. This leads to further distortion in helical confirmation and corroborates

the formation of zigzag chain configurations of polymer chains of PEO; (ii) reduction of GO to reduced graphene oxide (rGO) and increase of their dispersion rate within the matrix of electrolyte membranes [37]; (iii) increase of *C*-axis repeat distance (I_C) values between GO nano-sheets, since during the fabrication process, polar molecules of methanol can be absorbed by GO, thus orienting their dipole moment parallel to the *C*-axis of GO resulting in turn in an increase of I_C value; (iv) fibrils of crystalline PEO can wind or intercalate between GO nano-sheets in the gallery of GO nano-sheets, which allows the fibrils of PEO to form numerous (EO/GO) interfaces via the formation of chemical interactions with the various functional groups localized onto the GO surfaces [38]; and (v) note that graphene oxide nano-sheets are negatively charged in slightly acidic and basic conditions due to the surrounding surface carboxyl groups [39]; maybe this could lead to the occurrence of synergetic interactions between the negatively charged GO nano-sheets and carbonyl groups (C=O) of PVP via the formation of hydrogen bonds, and Na⁺ ions.

The Raman intensity ratio “ I_D/I_G ” provides the better information about in-plane crystallite size (L_a), which is useful

for understanding the intercalation tendency of the polymer chains and the interaction of cations within the gallery of GO nano-sheets [40]. Note that a large crystallite size of GO is a desirable parameter for GO-incorporated polymer electrolytes to realize their adaptability in high-performance metal ion batteries. The L_a values of all nanocomposite electrolyte membranes were determined using Tuinstra–Koenig relationship (Eq. 1) and from I_D/I_G data from Fig. 4 [41].

$$L_a(\text{nm}) = \frac{((2.4 \times 10^{-10}) \times \lambda_{\text{laser}}^4)}{(I_D/I_G)} \tag{1}$$

where λ_{laser} is the laser line wavelength in nm units and I_D, I_G are the peak intensities of D and G bands, respectively. Significantly, we observed a decreasing trend of L_a values from 40.68 to 30.71 nm upon increasing of GO weight percentage from 0.2 to 0.6 wt.% (Fig. 4). This evidences the steric stabilizing or capping nature of PVP, which hinders the π – π interactions between the GO nano-sheets and favors the uniform dispersion of GO nano-sheets associated with a decrease of shorter distance between defects on the plane of reduced GO nano-sheets. Consequently, an increase of the close proximity between GO surfaces and polymer chains must occur, tailoring the number in (EO/GO) interfaces.

UV-Vis spectroscopy

The optical absorption spectra of PEO/PVP/NaIO₄/GO (0, 0.2, 0.4 and 0.6 w/w) electrolyte membranes are presented in Fig. 5. Comparatively, nanocomposite electrolyte membranes exhibited relatively higher absorbance and the light absorbance was observed to be extended into the visible region (> 450 nm) with the increase of GO weight percentage. This evidences the successful incorporation of GO nano-sheets and their uniform distribution in the matrix of fabricated

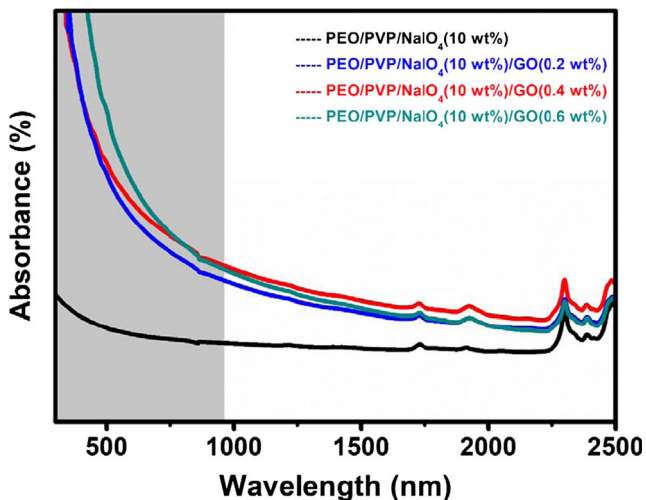


Fig. 5 Optical absorption spectra for different electrolyte membranes

nanocomposite electrolyte membranes [42]. In the present study, optical absorption edge, direct and indirect optical bandgap values of electrolyte membranes were determined by extrapolating the linear portions in the plots of $\alpha, (\alpha h\nu)^2$ and $(\alpha h\nu)^{1/2}$ versus photon energy ($h\nu$) (SMI, Fig. S2) [43, 44]. In reference to PEO/PVP/NaIO₄, GO-incorporated electrolyte membranes demonstrated a red shift of optical properties (direct, indirect band gap, and band edge position values) as a function of GO concentration (Table 2). This can be attributed to the formation of new localized states (associated to defects relative to the GO nano-sheets), which can extend into the highest occupied molecular orbital (HOMO) and the lowest unoccupied molecular orbital (LUMO) energy bands making the lower energy transitions reachable [45]. The enhanced optical absorbance and bandgap narrowing values of the present nanocomposite PEO/PVP/NaIO₄ electrolyte membranes suggest their adaptability as a key component for the applications in efficient light energy utilization. The Kubelka–Munk reflectance (R_C) values of nanocomposite electrolyte membranes were estimated by employing recorded UV-Vis-NIR diffuse reflectance spectra (DRS) (SMI, Fig. S3), estimated direct bandgap (E_g), refractive index (n) values, and Saunderson formula (Eq. 2), which is the modified form following the Kubelka–Munk model [46, 47]. Figure 6(i) shows the variation of R_C values as a function of wavelength for PEO/PVP/NaIO₄/GO (0, 0.2, 0.4, and 0.6 wt%) electrolyte membranes. In comparison to PEO/PVP/NaIO₄ electrolyte membrane, the nanocomposite PEO/PVP/NaIO₄/GO electrolyte membranes demonstrated higher optical absorption in the visible region; this could be attributed to the increasing in number of interfacial interactions between the various function groups on GO surfaces and the polymer chains of PEO/PVP blend.

$$R_m = k_1 + \frac{(1-k_1)(1-k_2)R_C}{(1-k_2R_C)} \tag{2}$$

where $R_m, k_1, k_2,$ and R_C are the measured reflectance, external reflectance, internal reflectance, and Kubelka–Munk reflectance, respectively. The external reflection (k_1) of the electrolyte membranes was mechanically eliminated by opening the specular exclusion port of the integrating sphere in the spectrophotometer. As a result, k_1 is equal to zero. The internal reflection k_2 was estimated from following expression [48], which provides the information regarding intrinsic optical responses from matrix of PEO/PVP/NaIO₄/GO electrolyte membranes.

$$k_2 = 0.3201 + 3.9779n^{-1} - 8.9452n^{-2} + 4.6952n^{-3} \tag{3}$$

Noteworthy, through the calculations of k_2 values derived from Eq. 3 (Fig. 6(ii)), an interesting trend was observed. Indeed, k_2 values increase upon increase of the weight concentration of GO

Table 2 Estimated optical band-edge, direct bandgap, and indirect bandgap values for nanocomposite electrolyte membranes

Sample	Optical edge (eV)	Direct bandgap (eV)	Indirect bandgap (eV)
PEO/PVP/NaIO ₄ (10 wt%)	3.69	3.62	3.2
PEO/PVP/NaIO ₄ (10 wt%)/GO (0.2 wt%)	2.76	2.65	2.58
PEO/PVP/NaIO ₄ (10 wt%)/GO (0.4 wt%)	2.69	2.64	2.54
PEO/PVP/NaIO ₄ (10 wt%)/GO (0.6 wt%)	2.31	2.22	2.13

nano-sheets. Clearly, the GO incorporation in the considered PEO/PVP/NaIO₄ polymeric blends does strongly reflect on the value of this coefficient, similar to the dramatic change in their optical absorption in the visible region, discussed above.

Thermal studies

Differential scanning calorimetry (DSC) and thermogravimetric analysis (TGA) studies were carried out for all fabricated electrolyte membranes to have a better understanding about

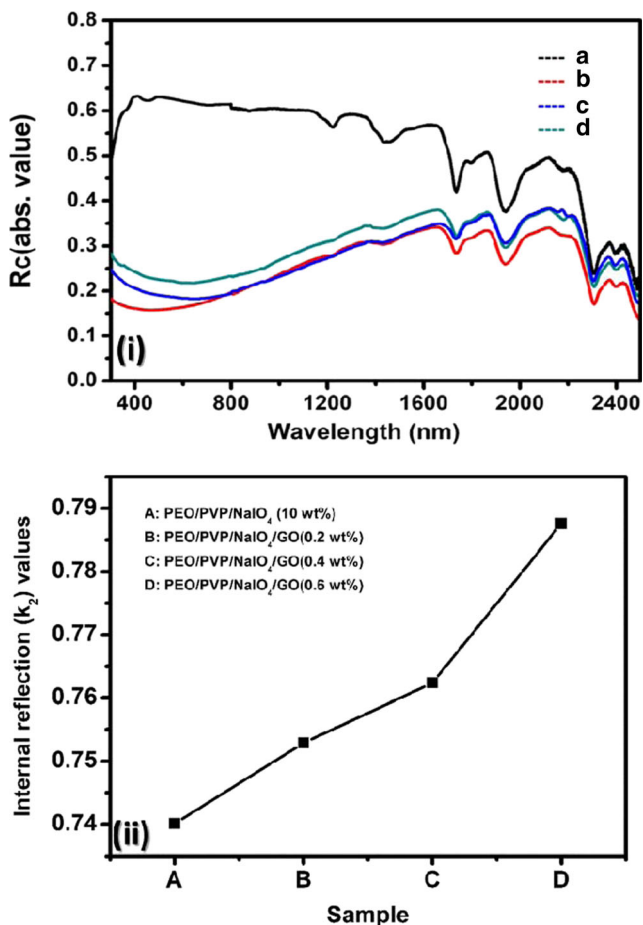


Fig. 6 Kubelka–Munk reflectance spectra for pure and nanocomposite electrolytes. (i) PEO/PVP (a), PEO/PVP/NaIO₄ (10 wt%) (b), PEO/PVP/NaIO₄ (10 wt%)/GO (0.2 wt%) (c), PEO/PVP/NaIO₄ (10 wt%)/GO (0.4 wt%) (d), and PEO/PVP/NaIO₄ (10 wt%)/GO (0.6 wt%) (e). (ii) Variation of determined internal reflection (k_2) values for nanocomposite electrolyte membranes as a function of GO concentration

their thermal stability properties. DSC experiments reveal the degree of crystallinity of the electrolytes and flexibility of their amorphous phases by evaluation of the melting (T_m) and glass transition (T_g) temperatures. It is well acquainted that room-temperature ionic conductivity of polymeric electrolyte membranes is usually related with a low degree of crystallinity and a high flexibility of the polymer host (i.e., low T_g values). Figure 7 presents the DSC curves obtained for PEO/PVP/NaIO₄ and GO (0.2, 0.4 and 0.6 w/w) incorporated PEO/PVP/NaIO₄ electrolyte membranes. The melting temperatures (T_m) were determined by considering the position of the dip of the endothermic peak, which can provide information on the melting of spherulite boundaries surfaces and on the state of crystallinity of the PEO matrix [49]. The glass transition temperature (DSC-onset, T_g) values were estimated by following extrapolation methods with respect to the baseline corrections (SMI, Fig. S4), providing the information of segmental motion of the polymer chains. In reference to PEO/PVP/NaIO₄ membrane, GO-incorporated electrolyte membranes displayed an increase of T_g , and melting enthalpy (ΔH_m) values and a slight decrease in their T_m values (Table 3). This can be interpreted as follows: in GO-loaded polymer electrolyte systems, segmental motion and mobility of polymer chains are predominantly depending on the close proximity of local environment of the round polymer chains

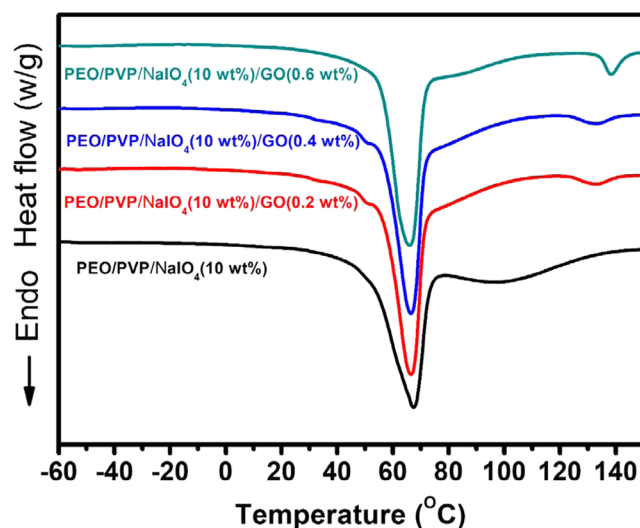


Fig. 7 DSC thermograms for GO-incorporated PEO/PVP/NaIO₄ (10 wt%) electrolyte membranes

Table 3 Glass transition, melting, decomposition, and crystallization temperatures of various polymer blend electrolytes

Sample	T_g (°C)	T_m (°C)	ΔH_m (J/g)	% χ_c	T_d (°C)
PEO/PVP/NaIO ₄ (10 wt%)	50.19	67.40	54.0	55.0	366.21
PEO/PVP/NaIO ₄ (10 wt%)/GO (0.2 wt%)	54.35	66.43	70.4	71.76	383.87
PEO/PVP/NaIO ₄ (10 wt%)/GO (0.4 wt%)	55.13	66.43	73.9	75.33	386.18
PEO/PVP/NaIO ₄ (10 wt%)/GO (0.6 wt%)	55.30	65.93	77.9	79.40	390.78

with the GO nanosheets through GO–polymer interfaces. The nature and strength of the GO–polymer interfaces may tailor the mobility of the polymer chains. Upon loading of GO nanosheets (0.2 wt%), the possible “polymers–GO” and “cation–GO” interactions create a tendency to form a high number of GO/EO interfaces. Note that GO/PVP interactions reduce the stacking tendency of GO nano-sheets and more number of hydroxyl groups in reduced GO leading to an increase in hydrogen bonding formation hence possible interfaces between GO and polymeric matrix. These quite strong hydrogen bonds would support the high content of PEO fibrils to intercalate into the gallery of GO and for the formation of crucial GO/EO interfaces. We supposed that the attractive nature of GO/EO interfaces could increase the tentatively packing density of PEO chains between GO nano-sheets and tends to decrease the fractional-free volume. This restricts the segmental motion of PEO backbone and mobility of polymer chains in amorphous portion, and thus raise in the T_g and ΔH_m values [50]. Generally, inclusion of GO nano-sheets enhances the salt dissociation rate and facilitates more number of salt ions. This favors for the dramatic increment of transient cross-link formations of Na⁺ ions with intercalated EO of PEO in the gallery of GO and reduces the surface-free energies of spherulite boundaries that will consequently melt at lower temperatures.

The TGA thermograms of all fabricated electrolyte membranes were recorded (Fig. 8) and the variation of decomposition temperatures (T_d) at 10 wt% weight loss were observed in the temperature range of 320–350 °C. Initial weight losses at 50 and 95 °C were noticed due to the evaporation of moisture in the samples [51]. In reference to PEO/PVP/NaIO₄ electrolyte membrane, the weight loss curves associated to the nanocomposite electrolyte membranes demonstrated two major stages of decomposition: (i) first, the weight loss in the temperature range of 100–130 °C, which could be owned to the de-intercalation of fibrils of PEO from the gallery of GO leading to decarboxylation; (ii) the second stage from 150 to 400 °C could be owing to the decomposition of oxygen functional groups on GO sheets and due to degradation of polymer blend to the decomposition of the GO framework and/or the degradation of the blended polymers [52, 53]. Significantly, the position of weight loss curves corresponding to the GO nano-sheets incorporated blend electrolytes were noticed to shift toward a higher temperature region (Table 3) in agreement with the instauration of strong interfacial interaction between GO nano-sheets (comprising outstanding mechanical properties, high flexibility, high bonding potential, and extremely high aspect ratios) and blended polymer. This contributes to increase the stiffness of intercalated polymer chains

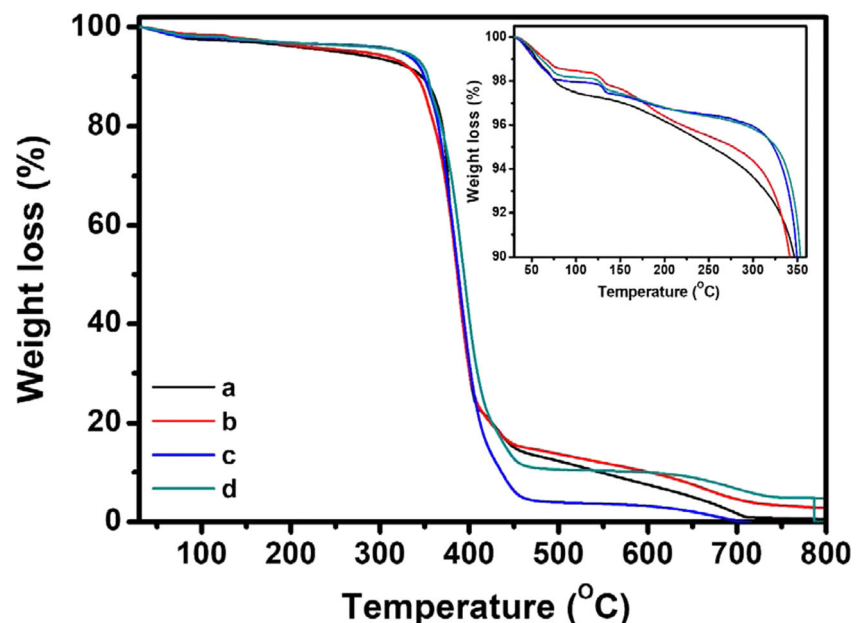
Fig. 8 Thermogravimetric analysis curves for nanocomposite electrolyte membranes. (a) PEO/PVP/NaIO₄ (10 wt%), (b) PEO/PVP/NaIO₄/GO (0.2 wt%), (c) PEO/PVP/NaIO₄/GO (0.4 wt%), and (d) PEO/PVP/NaIO₄/GO (0.6 wt%)

Table 4 Estimated average Young's modulus (E , MPa), tensile strength (S_{ut} , MPa), and ductility values for nanocomposite polymer electrolyte membranes as a function of graphene oxide (GO) concentration

Sample	E (MPa)	S_{ut} (MPa)	Ductility (%)
PEO/PVP/NaIO ₄ (10 wt%)	418.8	5.23	1.83
PEO/PVP/NaIO ₄ (10 wt%)/GO (0.2 wt%)	551.6	8.15	2.08
PEO/PVP/NaIO ₄ (10 wt%)/GO (0.4 wt%)	702.4	8.98	1.61
PEO/PVP/NaIO ₄ (10 wt%)/GO (0.6 wt%)	661.7	5.33	1

into the gallery of GO and thus increase the range of decomposition temperatures of nanocomposites with an increase of GO concentration. With respect to PEO/PVP/NaIO₄ electrolyte, the position of weight loss curve associated to nanocomposite PEO/PVP/NaIO₄/GO (0.6% in weight) electrolyte membrane demonstrated a maximum shift of 24.8 °C toward higher temperature region on temperature axis. In addition to this, an extended plateau region between 150 and 350 °C evidences for the enhancement in thermal stability of fabricated nanocomposite electrolyte membranes in the present study.

Mechanical properties

Mechanical stability properties of SPEs are significant to overcome the drawbacks from liquid-state electrolytes and to improve the durability by expanding the operating conditions of

electrochemical cells. Graphene-based derivatives are recognized as ideal nano-filler components, owing to their exceptional mechanical properties and flexible in nature, for the fabrication of multi-functional polymer nanocomposites with more toughness [54]. In this context, incorporation of graphene oxide components into various polymer matrices might result in a dramatic improvement in the mechanical properties such as elastic modulus, tensile strength, and toughness. Most of the work that reported on mechanical stability properties of polymers incorporating GO nano-fillers have been performed for pure PEO matrices [55–57]. The mechanical properties of PEO/PVP blend-based electrolyte membranes have not yet been reported, even though these properties are crucial for SPEs for the fabrication of sodium ion (Na⁺) batteries. Mechanical stability tests were carried out, up to the fracture, for all fabricated membranes to determine

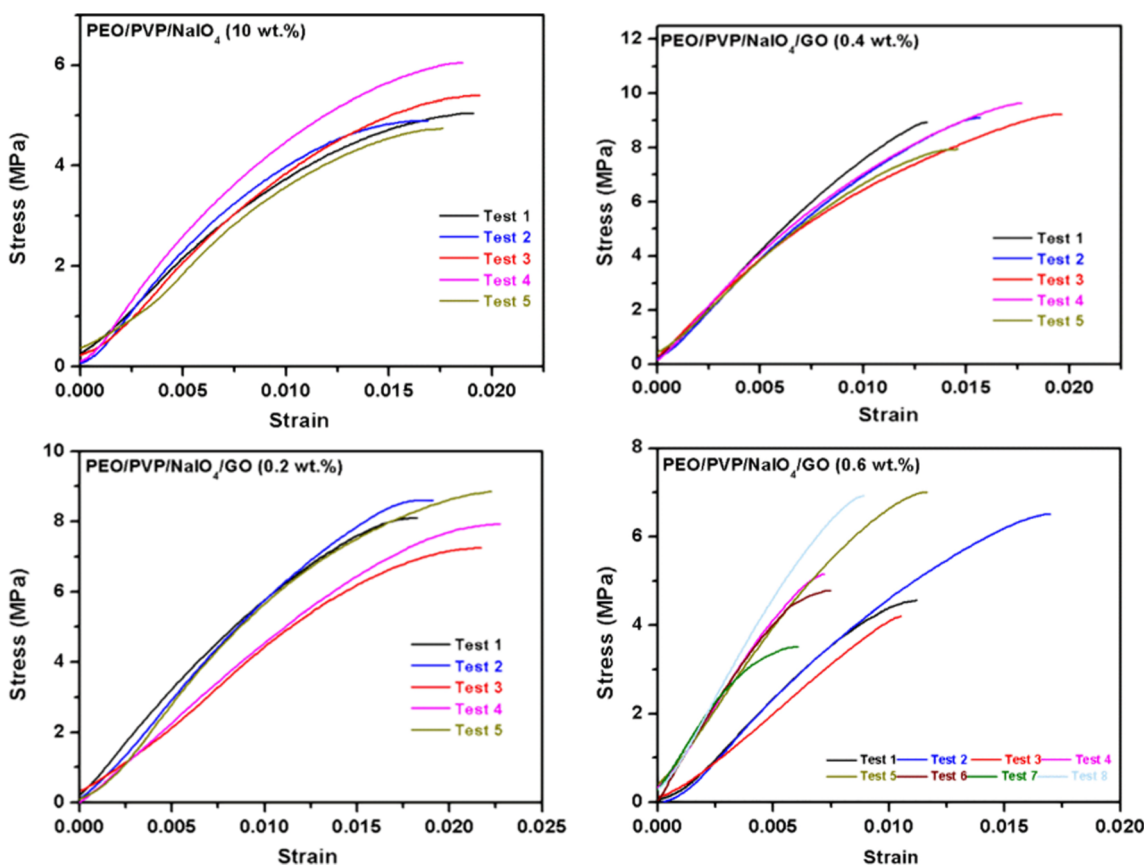


Fig. 9 Stress–strain curves for nanocomposite PEO/PVP/NaIO₄ electrolyte membranes

their tensile strength, their Young's modulus, and ductility properties and obtained data are summarized in Table 4. Figure 9 shows stress-strain curves for all present electrolyte membranes. The PEO/PVP/NaIO₄ electrolyte membrane demonstrated an average tensile strength of 5.23 MPa, Young's modulus of 418.8 MPa, and displayed the ductility of 1.83%. Comparatively, GO nano-sheets incorporated PEO/PVP/NaIO₄ electrolyte membranes demonstrated improved mechanical stability properties. In the present study, PEO/PVP/NaIO₄/GO (0.4 wt.%) electrolyte membrane demonstrated improved tensile strength of 41.8% and Young's modulus of 40.4% and displayed a maximum fractured elongation of 3%. This can be interpreted as follows: (i) the strong confinement of polymer chains/GO interfaces, (ii) unique chemical cross-linking between the carboxyl functional groups primarily located around the edge of the GO nano-sheet and functional groups onto the polymer chains related to PEO/PVP blend via multiple strengthening mechanisms: hydrogen bonding, entropic elasticity of the polymeric chains, covalent bonding between the graphene oxide and polymer chains; and (iii) increased specific interracial area due to dispersion of GO nano-sheets (of 0.4% in weight) in the matrix of PEO/PVP/NaIO₄ electrolyte [58, 59]. In opposition, doping with higher concentration of GO (> 0.4 wt.%) leads to decrease in the mechanical stability of PEO/PVP/NaIO₄ electrolytes. This could be due to poor dispersion and excessive aggregation or stacking of GO sheets and/or diffusion tortuosity.

Impedance spectroscopy

Figure 10 shows typical Nyquist plots of nanocomposite polymer electrolytes embedded with three different concentrations of GO nano-sheets. Each Nyquist plot consists of a depressed semicircle toward the higher frequency of the applied electric field. The feature is followed by a spike at the lower frequency

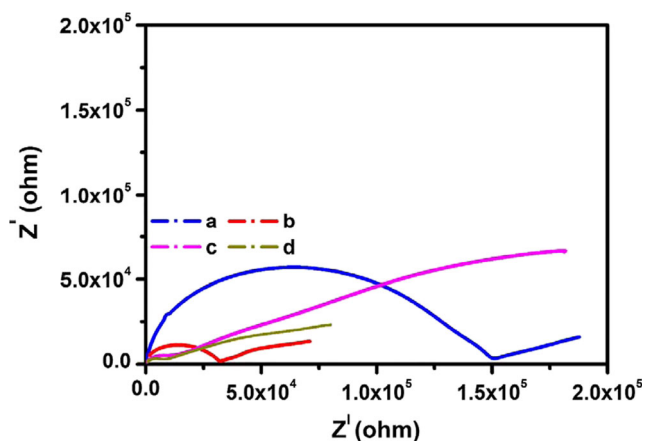


Fig. 10 Nyquist plots for GO-incorporated electrolyte membranes. (a) PEO/PVP/NaIO₄ (10 wt%), (b) PEO/PVP/NaIO₄ (10 wt%)/GO (0.2 wt%), (c) PEO/PVP/NaIO₄ (10 wt%)/GO (0.4 wt%), and (d) PEO/PVP/NaIO₄ (10 wt%)/GO (0.6 wt%)

side. The depressed semicircle represents the conductive properties of the bulk material while the tilted spike represents the electrical double layer [60]. The bulk resistance (R_b) is determined from the point of intersection of higher end of semicircle with the real ($Z^l = R_b$) axis. The room temperature ionic conductivities of all present electrolytes were calculated using the expression $\sigma = t / (R_b * A)$, where t and A are the thickness and effective area of the electrolyte membranes, respectively [61]. The estimated room temperature ionic conductivity of pure PEO/PVP/NaIO₄ (10 wt%) electrolyte membrane was found to be 1.56×10^{-7} S/cm [27] and observed meager increment in room-temperature ionic conductivity as a result of addition of GO nano-sheets (0.2, 0.4, and 0.6 wt%). In the present study, PEO/PVP/NaIO₄/GO (0.6 wt.%) electrolyte membrane exhibited higher room-temperature conductivity of 1.89×10^{-6} S/cm. This could be attributed to synergistic interactions between GO/polymer chains or GO/Na⁺ ions, which leads to restrict the segmental motion of polymer chains, mobility of Na⁺ ions, and/or finding a new site on PEO polymer chains during the hopping mechanism of Na⁺ ions [62].

Conclusions

The nanocomposite PEO/PVP/NaIO₄/GO solid polymer electrolyte membranes were successfully fabricated using solution casting technique. A unique surface morphology comprising circular-shaped protuberances of different dimensions revealed the inlaid clusters of GO nano-sheets and their exfoliation in the matrices of nanocomposite polymer electrolytes. The incorporation of GO nano-additives in PEO/PVP/NaIO₄ blends resulted in suppression of all characteristic Raman bands related to PEO and PVP polymers. The increase of the ratio of Raman intensities (I_D/I_G) related to D and G bands and a decrease of in-plane crystallite size (L_a) values are attributed to the successful incorporation and good distribution of GO nano-sheets. A characteristic red shift and improved light absorption in the visible region evidenced for the inclusion of GO nano-sheets and the interfacial interactions of GO/polymer chains in the matrices of PEO/PVP/NaIO₄/GO electrolytes. The nanocomposite PEO/PVP/NaIO₄/GO electrolytes demonstrated excellent thermal stability properties as evidenced by a plateau region between 150 and 350 °C. Significantly, with respect to PEO/PVP/NaIO₄ electrolyte, the nanocomposite PEO/PVP/NaIO₄/GO (0.4% in weight) electrolyte membrane demonstrated improved tensile strength of 41.8% and Young's modulus of 40.4%. The PEO/PVP/NaIO₄/GO (0.6 wt.%) electrolyte membrane demonstrated higher room temperature conductivity of 1.89×10^{-6} S/cm with appreciable mechanical properties (tensile strength of 8.98 MPa, Young's modulus of 702 MPa) with respect to PEO/PVP/NaIO₄ electrolyte.

Acknowledgements The author gratefully acknowledges the INERA EU project Research Potential “Research and Innovation Capacity Strengthening of ISSP-BAS in Multifunctional Nanostructures” (FP7 REGPOT-2012-2013-1) support.

Compliance with ethical standards

Conflict of interest We confirm that this manuscript has not been published elsewhere and is not under consideration by another journal and we have no conflicts of interest to disclose.

References

- Tarascon JM, Armand M (2001) Issues and challenges facing rechargeable lithium batteries. *Nature* 414:359–367
- Kim SK, Kim DG, Lee A, Sohn HS, Wie JJ, Nguyen NA, Mackay ME, Lee JC (2012) Organic/inorganic hybrid block copolymer electrolytes with Nanoscale ion-conducting channels for lithium ion batteries. *Macromolecules* 45:9347–9356
- Li XH, Yu YF, Liu QF, Meng YZ (2012) Synthesis and properties of anion conductive Ionomers containing Tetrphenyl methane moieties. *ACS Appl Mater Interfaces* 4:3627–3635
- Chen HG, Wang SJ, Xiao M, Meng YZ (2007) Novel sulfonated poly(phthalazinone ether ketone) ionomers containing benzonitrile moiety for PEM fuel cell applications. *J Power Sources* 165:16–23
- Xu K (2014) Electrolytes and interphases in Li-ion batteries and beyond. *Chem Rev* 114:11503–11618
- Yuan M, Erdman J, Tange C, Ardebili H (2014) High performance solid polymer electrolyte with graphene oxide nanosheets. *RSC Adv* 4:59637–59642
- Bar N, Basak P, Tsur Y (2017) Vibrational and impedance spectroscopic analyses of semi-interpenetrating polymer networks as solid polymer electrolytes. *Physics chemistry. Chem Phys* 19:14615–14624
- Stephan AM (2006) Review on gel polymer electrolytes for lithium batteries. *Eur Polym J* 42:21–42
- Bresser D, Oschmann B, Tahir MN, Mueller F, Lieberwirth I, Tremel W, Zentel R, Passerini S (2015) Carbon-coated Anatase TiO₂ nanotubes for li- and Na-ion anodes. *J Electrochem Soc* 162(2):A3013–A3020
- Zheng Q, Ma L, Khurana R, Archer LA, Coates GW (2016) Structure-property study of cross-linked hydrocarbon/poly(ethylene oxide) electrolytes with superior conductivity and dendrite resistance. *Chem Sci* 7:6832–6838
- Spindler R, Shriver DF (1986) Physical and spectroscopic properties of ternary polymer electrolytes composed of poly(vinylpyrrolidinone), polyethylene glycol, and lithium trifluoromethanesulfonate. *Macromolecules* 19:347–350
- Agrawal RC, Pandey GP (2008) Solid polymer electrolytes: materials designing and all-solid-state battery applications: an overview. *J Phys D Appl Phys* 41:223001
- Scrosati B, Vincent CA (2000) Polymer electrolytes: the key to lithium Polymer batteries. *MRS Bull* 25:28–30
- Balazs AC, Emrick T, Russell TP (2006) Nanoparticle polymer composites: where two small worlds meet. *Science* 314:1107–1110
- Mackay ME, Tuteja A, Duxbury PM, Hawker CJ, Horn BV, Guan Z, Chen G, Krishnan RS (2006) General strategies for nanoparticle dispersion. *Science* 311:1740–1743
- Warren SC, Disalvo FJ, Wiesner U (2007) Nanoparticle-tuned assembly and disassembly of mesostructured silica hybrids. *Nat Mater* 6:156–161
- Akhtar MS, Kwon S, Stadler FJ, Yang OB (2013) High efficiency solid state dye sensitized solar cells with graphene-polyethylene oxide composite electrolytes. *Nano* 5:5403–5411
- Moniruzzaman M, Karen IW (2006) Polymer nanocomposites containing carbon nanotubes. *Macromolecules* 39:5194–5205
- Kotov N A, D’ek’any I and Fendler J H (1996) Ultra graphite oxide-polyelectrolyte composites prepared by self-assembly: transition between conductive and non-conductive states. *Adv Mater* 8: 637–641
- Paci JT, Belytschko T, Schatz GC (2007) Computational studies of the structure, behavior upon heating, and mechanical properties of graphite oxide. *Journal of Physics Chemistry C* 111:18099–18111
- Corcione CE, Frigione M (2012) Characterization of nanocomposites by thermal analyses. *Materials* 5:2960–2980
- Shim J, Kim D, Kim HJ, Lee JH, Baik J, Lee J (2014) Novel composite polymer electrolytes containing poly(ethylene glycol)-grafted graphene oxide for all-solid-state lithium-ion battery applications. *J Mater Chem A* 2:13873–13883
- Gao S, Zhong J, Xue G, Wang B (2014) Ion conductivity improved polyethylene oxide/lithium perchlorate membranes modified by graphene oxide. *J Membr Sci* 470:316–322
- Young W-S, Kuan W-F, Epps TH (2014) Block copolymer electrolytes for rechargeable lithium batteries. *J Polym Sci B Polym Phys* 52:1–16
- Vignarooban K, Kushagra R, Elango A, Badami P, Mellander B-E, Xu X, Tucker TG, Nam C, Kannan AM (2016) Current trends and future challenges of electrolytes for sodium-ion batteries. *Int J Hydrog Energy* 41:2829–2846
- Chen J, Huang Z, Wang C, Porter S, Wang B, Lie W, Liu HK (2015) Sodium-difluoro(oxalate) borate (NaDFOB): a new electrolyte alt for Na-ion batteries. *Chem Commun* 51:9809–9812
- Koduru HK, Marino L, Scarpelli F, Petrov AG, Marinov YG, Hadjichristov GB, Iliiev MT, Scaramuzza N (2017) Structural and dielectric properties of NaIO₄-complexed PEO/PVP blended solid polymer electrolytes. *Curr Appl Phys* 17:1518–1531
- Zhang SP, Xiong P, Yang XJ, Wang X (2011) Novel PEG functionalized graphene nanosheets: enhancement of dispensability and thermal stability. *Nano* 3:2169–2174
- Takahashi Y and Tadokoro H (1973) Structural studies of polyethers, -(CH₂)_m-O-_n-X. Crystal structure of poly(ethylene oxide). *Macromolecules* 6:672–675
- Cao Y-C, Xu C, Wu X, Wang X, Xing L, Scott K (2011) A poly(ethylene oxide)/graphene oxide electrolyte membrane for low temperature polymer fuel cells. *J Power Sources* 196:8377–8382
- Hackett E, Manias E, Giannelis EP (2000) Computer simulation studies of PEO/layer silicate nanocomposites. *Chem Mater* 12: 2161–2167
- Maxfield J, Shepherd IW (1995) Confirmation of poly(ethylene xide) in the solid state, melt and solution measured by Raman scattering. *Polymer* 16:505–509
- Yoshihara T, Tadokoro H, Murahashi S (1964) Normal vibrations of the polymer molecules of helical conformation. IV. Polyethylene oxide and polyethylene-d₄ oxide. *J Chem Phys* 41:2902–2911
- Fang M, Wang K, Lu H, Yang Y, Nutt S (2010) Single-layer graphene nanosheets with controlled grafting of polymer chains. *J Mater Chem* 20:1982–1992
- Zhang X, Wang J, Jia H, Yin B, Ding L, Xu Z, Ji Q (2016) Polyvinyl pyrrolidone modified graphene oxide for improving the mechanical, thermal conductivity and solvent resistance properties of natural rubber. *RCS Advances* 6:54668–54678
- Pimenta MA, Dresselhaus G, Dresselhaus MS, Cancado LG, Jorio A, Saito R (2007) Studying disorder in graphite-based systems by Raman spectroscopy. *Physics chemistry. Chem Phys* 9:1276–1291
- Stankovich S, Dikin DA, Piner RD, Kohlhaas k A, Kleinhammes A, Jia Y, Wu Y (2007) Synthesis of graphene-based nanosheets via

- chemical reduction of exfoliated graphite oxide. *Carbon* 45:1558–1565
38. Shen J, Shi M, Yan B, Ma H, Li N, Ye M (2011) Ionic liquid-assisted one-step hydrothermal synthesis of TiO₂-reduced graphene oxide composites. *Nano Res* 4:795–806
 39. Hu K, Kulkarni DG, Choi I, Tsukruk VV (2014) Graphene-polymer nanocomposites for structural and functional applications. *Prog Polym Sci* 39:1934–1972
 40. Swain AK, Bahadur D (2014) Enhanced stability of reduced Graphene oxide colloid using cross-linking polymers. *J Phys Chem C* 118:9450–9457
 41. Cancado L, Takai K, Enoki T, Endo M, Kim YA, Mizusaki H, Jorio A, Coelho L N, Magalhães-Paniago R and Pimenta M A (2006) General equation for the determination of the crystallite size L_a of nanographite by Raman spectroscopy. *Appl Phys Lett* 88: 163106
 42. Chen D, Zou L, Li S, Zheng F (2016) Nanospherical like reduced graphene oxide decorated TiO₂ nanoparticles: an advanced catalyst for the hydrogen evolution reaction. *Sci Rep* 6:20335 (1–8)
 43. Davis PW, Shalliday TS (1960) Some optical properties of cadmium telluride. *Phys Rev* 118:1020–1022
 44. Thutupalli GKM, Tomlin SG (1976) The optical properties of thin films of cadmium and zinc selenides and tellurides. *J Phys D Appl Phys* 9:1639–1646
 45. Al-Ramadin Y (2000) Optical properties of poly(vinyl chloride)/poly(ethylene oxide). *Opt Mater* 14:287–290
 46. Saunderson JL (1942) Calculation of the color of pigmented plastics. *Journal of Optical Society of America* 32:727–736
 47. Mudgett PS, Richards LW (1973) Kubella-Munk scattering and absorption coefficients for use with glossy, opaque objects. *Journal of Painting Technology* 45:44–53
 48. Wen-Dar HO, Chen-Chi MMA, Lieh-Chun WU (1998) Diffuse reflectance and transmittance of IR absorbing polymer film. *Polym Eng Sci* 38:1666–1674
 49. Bandara TMWJ, Mellander B-E, Albinsson I, Dissanayake MAKL, Pitawala HMJC (2009) Thermal and dielectric properties of PEO/EC/Pr4N+I- polymer electrolytes for possible applications in photo-electro chemical solar cells. *J Solid State Electrochemistry* 13:1227–1232
 50. Cheng HKF, Sahoo NG, Tan YP, Pan YZ, Bao HQ, Li L, Chan SH, Zhao JH (2012) Poly(vinyl alcohol) nanocomposites filled with poly(vinyl alcohol)-grafted graphene oxide. *ACS Appl Mater Interfaces* 4:2387–2394
 51. Stephan AM, Saito Y, Muniyandi N, Renganathan NG, Kalyanasundaram S, Elizabeth RN (2002) Preparation and characterization of PVC/PMMA blend polymer electrolytes complexed with LiN(CF₃SO₂)₂. *Solid State Ionics* 148:467–473
 52. Niu Y, Fang Q, Zhang X, Zhang P, Li Y (2016) Reduction and structural evolution of graphene oxide sheets under hydrothermal treatment. *Phys Lett A* 380:3128–3132
 53. Noor SAM, Ahmad A, Talib IA, Rahman MYA (2010) Morphology, chemical interaction, and conductivity of a PEO-ENR50 based on solid polymer electrolyte. *Ionics* 16:161–170
 54. Cassagneau T, Fendler JH (1998) High density rechargeable lithium-ion batteries self-assembled from graphite oxide nanoplatelets and polyelectrolytes. *Adv Mater* 10:877–881
 55. Wang W and Alexandridis P (2016) Composite polymer electrolytes: nanoparticles affect structure and properties. *Polymers* 8(11): 387 (1–36)
 56. Klongkan S, Pumchusak J (2015) Effects of the addition of LiCF₃SO₃ salt on the conductivity, thermal and mechanical properties of PEO-LiCF₃SO₃ solid polymer electrolyte. *International Journal of Chemical Engineering and Applications* 6:165–168
 57. Ji J, Li B, Zhong W-H (2010) Simultaneous enhancing ionic conductivity and mechanical properties of solid polymer electrolytes via a copolymer multi-functional filler. *Electrochimica Acta* 55: 9075–9082
 58. Tian Y, Cao Y, Wang Yu YW, Feng J (2013) Realizing ultra modulus and high strength of macroscopic graphene oxide papers through crosslinking of mussel-inspired polymers. *Adv Mater* 25: 2980–2983
 59. Cheng Q, Wu M, Li M, Jiang I, Tang Z (2013) Ultratough artificial nacre based on conjugated cross-linked graphene oxide. *Angew Chem Int Ed* 52:3750–3755
 60. Kim SK, Miyayama M, Yanagida H (1995) Electrical anisotropy and a plausible explanation for dielectric anomaly of Bi₄Ti₃O₁₂ single. *Mater Res Bull* 31:121–131
 61. Nguyen CA, Xiong S, Ma J, Lu X, Lee PS (2011) High ionic conductivity P(VDF-TrFE)/PEO blended polymer electrolytes for solid electrochromic devices. *Phys Chem Chem Phys* 13:13319–13326
 62. Dreyer DR, Park S, Bielawski CW, Ruoff RS (2010) The chemistry of graphene oxide. *Chem Soc Rev* 39:228–240